Electronic Supplementary Material (ESI) for Journal of Materials Chemistry A.

Supporting Information

Design of Ni_3N/Co_2N heterojunction for boosting electrocatalytic alkaline overall water splitting

Yan Wen, Jingyao Qi*, Peicheng Wei, Xu Kang, and Xin Li*

1. Methods

1.1 Synthesis of NiCo-LDH material.

The NiCo layered double hydroxide (denoted as NiCo-LDH) was synthesized by the hydrothermal method. Nickel foam substrate (1 cm × 3 cm) was cleaned by HCl solution (5 wt%) for 10 min to remove the surface nickel oxide layer and then cleaned by deionized water and acetone for 20 min each time. All operations are performed in an ultrasonic water bath and the products were dried at 60°C for further use. $Ni(NO_3)_2 \cdot 6H_2O$ (6 mmol), $Co(NO_3)_2 \cdot 6H_2O$ (6 mmol), and CH_3COONa (12 mmol) were dissolved in 40 mL of deionized water and stirred for 30 min for a homogenous solution. Then, the above solution and Nickel foam substrate were transferred into a 50 mL Teflon liner hydrothermal reactor and maintained at 120°C for 10h. Cooling to room temperature naturally and rinsed with deionized water and ethanol three times. The product NiCo-LDH was prepared. The sample was dried in a vacuum oven at 60°C for 12h.

1.2 Synthesis of N drop NiCo-LDH material.

The as-prepared NiCo-LDH was transferred to a tube furnace. The composite sample was subjected to pyrolysis under pure ammonia flow by programmatically ramping the temperature from room temperature to 300°C at a rate of 10°C min^{-1} for 6h. After the reaction was completed, the product was washed with deionized water and ethanol several times and dried in a vacuum oven at 60°C overnight. The pyrolyzed sample was denoted as N-NiCo-LDH-6. Similarly, N-NiCo-LDH-2, N-NiCo-LDH-4, and N-NiCo-LDH-8 were synthesized with the same synthesis strategy except for the pyrolysis time (2, 4, and 8 h, respectively).

1.3 Structural Characterizations.

The morphology of all the samples was characterized by scanning electron microscope (SEM, S4800 HSD electron microscopy, Hitachi) and transmission electron microscopy (TEM, Tecnai G2 F20 electron micros-cope, FEI). The N_2 isotherm adsorption/desorption (N_2-IAD) was implemented by the Brunauer–Emmett–Teller (BET) method using the micropore physisorption analyzer (NOVAtouch, Anton-Paar). The crystalline structure was tested by the X-ray powder diffraction (XRD) spectrum on an X-

ray diffractometer (XRD, Empyrean, Panalytical) with Cu Ka radiation (λ= 0.1504 nm). The elemental composition and content of the as-synthesized samples were collected on X-ray photoelectron spectroscopy (XPS, ESCALAB 250Xi, ThermoFisher).

1.4 Electrochemical Characterizations.

Electrocatalytic activity measurements were carried out on an electrochemical workstation (CHI 660E, Chenhua, Shanghai) with a three-electrode system in 1 M KOH aqueous solution, where a Hg/HgO electrode (1.0 M KOH, CH Instruments) and a graphite rod (3 mm in diameter) were used as the reference electrode and the counter electrode, respectively. Before the test, the electrolyte in the reaction cell was saturated with N_2 flow for 30 min and the sample was activated by 60 cycles of cyclic voltammetry scanning. All polarization curve results were calibrated by the 95% *iR*-Correction unless otherwise specified. The polarization curves were measured by the linear sweep voltammetry (LSV) at 2 mV·s^{-1}. We obtained the Tafel slope by recording the overpotential vs. $\log_{10}|j|$ and fitting the linear portions at low overpotential to the Tafel equation:

$$\eta = a + b\log_{10}|j| \tag{1}$$

Where j is the cathodic current density, η is the overpotential and b is the Tafel slope.

The electrochemical impedance spectroscopy (EIS) measurements were carried out from 10^6 to 10^{-1} Hz in potentiostatic mode with a sinusoidal AC potential amplitude of 5 mV.

The conductivity of catalysis can be cauculated by the following equation:

$$\sigma = \frac{1}{\rho} \tag{2}$$

$$R = \frac{\rho L}{S} \tag{3}$$

Where R is the resistance of electrode. L is the geometric length of electrode. S is geometry surface area of electrode. ρ is the resistivity and σ is the conductivity of electrode.

The double layer capacitance (C_{dl}) was determined by the CV method at the non-faradaic potentials from 0.2 to 0.3 V vs. RHE. The scan rate range of CV was from 20 to 100 mV s^{-1}. Stability measurements were carried out by 3000 cycles of CV scanning and

long-term stability tests were performed under a constant current density of 10 $mA \cdot cm^{-2}$. All measured potentials were converted to the reversible hydrogen electrode (RHE) by the Nernst equation. The prepared materials are immersed in the sodium dihydrogen phosphate of different concentrations to verify the electrochemically active sites of the materials. Sodium dihydrogen phosphate solution concentration changes from 0.1 M to 2 M. Electrode immersion time was 5 min. The immersed electrodes were washed, dried, and then tested under the above operating conditions. The electrolytic overall water splitting was performed in a two-electrode system in 1 M KOH aqueous solution in which as-prepared electrode materials as bifunctional electrocatalysts.

1.5 Theoretical calculation details

We performed the first-principles calculations on Vienna ab initio simulation packages (VASP) plane-wave package with Perdew-Burke-Ernzerhof (PBE) functional. The energy cut-off value of the plane-wave basis was 450 eV. The generalized gradient approximation (GGA) was used to describe the electronic exchange and correlation effects and the KP-Resolved valure is 0.04 for generating the K-Mesh. the vacuum layer of 15 Å for supercell was used to avoid the interaction between the layers. The Self-consistent iteration was converged until the force of each atom was less than 0.05 eV $Å^{-1}$ and the total energy convergence criterion of 1×10^{-5} eV. After structural optimization, the density of states analysis (DOS) was performed, in which the force tolerance of 0.03 eV $Å^{-1}$ and the energy tolerance of 1×10^{-6} eV per atom was considered.

For OER process, the Gibbs free energy calculated was divided into four reaction paths (R1~R4):

$$R1: * + H_2O = *OH + H^+ + e^-$$

$$R2: *OH = *O + H^+ + e^-$$

$$R3: *O + H_2O = *OOH + H^+ + e^-$$

$$R4: *OOH = * + O_2 + H^+ + e^-$$

For HER process. the Gibbs free energy calculated follow the reaction R5:

$$R5: * + H_2O + e^- = OH^- + *H$$

Where * stands for the active site on the catalytic surface. Gibbs free energy can be calculated as follows equations (4) ~ (8):

$$\Delta G_{R1} = E(*OH) + E(H_2)/2 + eU - E(*) - E(H_2O) + \Delta(ZPE - T\Delta S) \quad (4)$$

$$\Delta G_{R2} = E(*O) + E(H_2)/2 + eU - E(*OH) + \Delta(ZPE - T\Delta S) \quad (5)$$

$$\Delta G_{R3} = E(*OOH) + E(H_2)/2 + eU - E(*O) - E(H_2O) + \Delta(ZPE - T\Delta S) \quad (6)$$

$$\Delta G_{R4} = E(O_2) + E(H_2)/2 + E(*) + eU - E(*OOH) + \Delta(ZPE - T\Delta S) \quad (7)$$

$$\Delta G_{*H} = E(*H) + E(OH^-) - E(*) - E(H_2O) - eU + \Delta(ZPE - T\Delta S) \quad (8)$$

Each energy was corrected by the zero-point energy (ZPE) and entropy (S). S was obtained by the phonon vibration frequency. T is 298.15 K.

2. Supplementary Figures

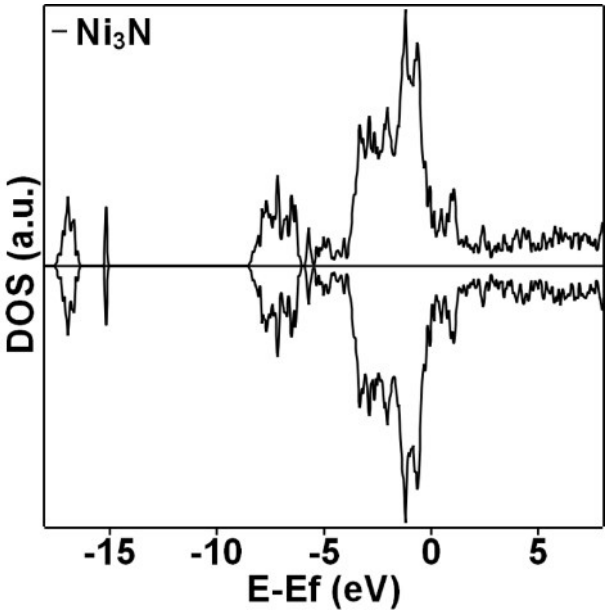

Fig.S1 Density of states on Ni_3N.

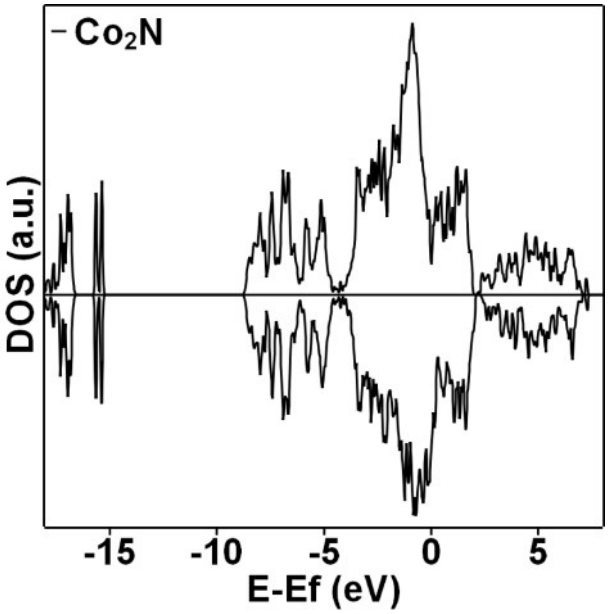

Fig.S2 Density of states on Co_2N.

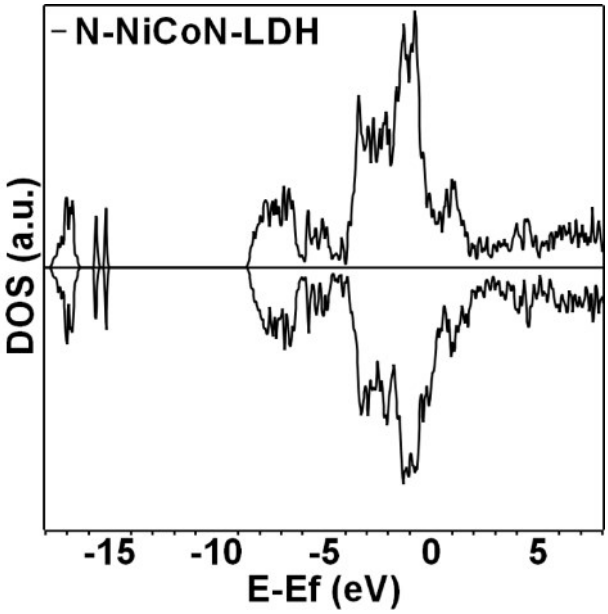

Fig.S3 Density of states on N-NiCo-LDH.

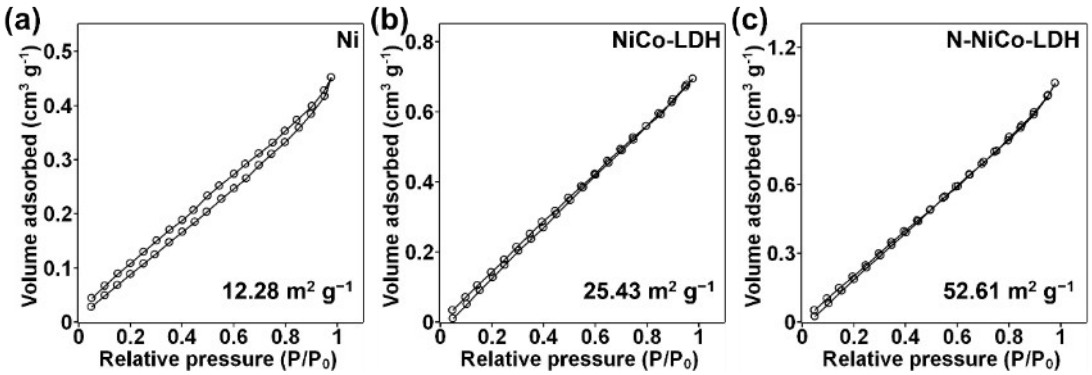

Fig.S4 N_2 IAD curve of Ni foam, NiCo-LDH, and N-NiCo-LDH.

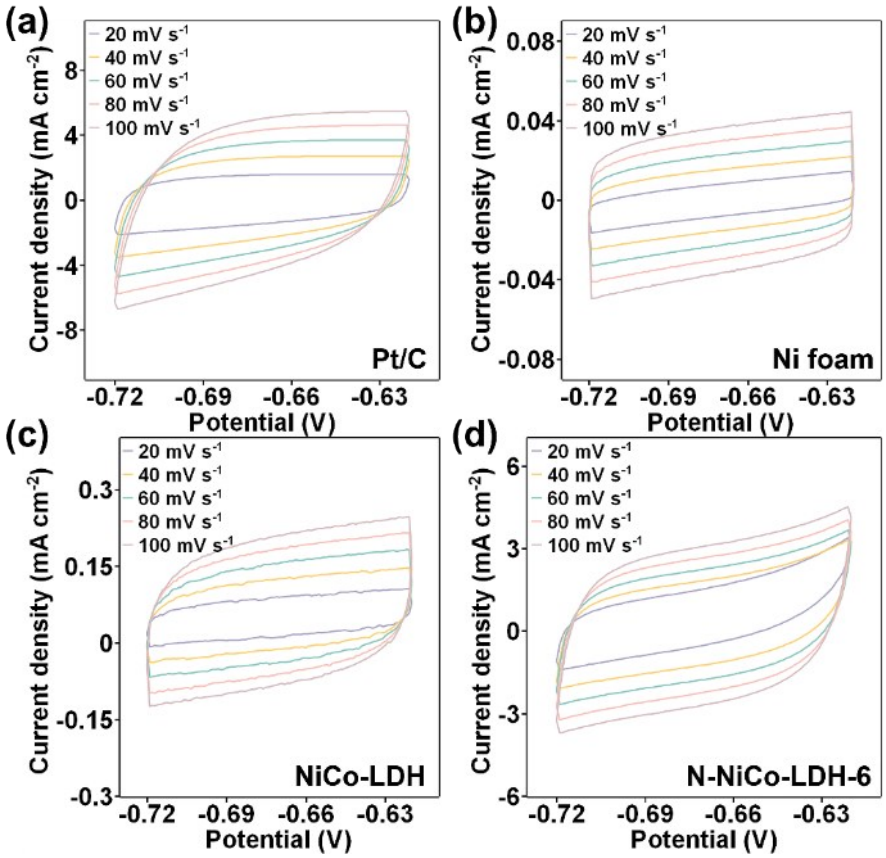

Fig.S5 Cyclic voltammograms of (a) Pt/C, (b) Ni foam, (c) NiCo-LDH and (d) N-NiCo-LDH-6 at scan rates from 20 to 100 mV·s^{-1}.

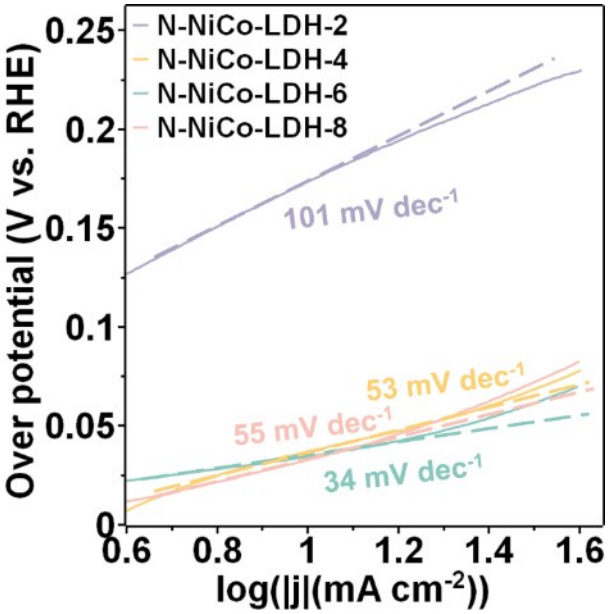

Fig.S6 HER Tafel plots of N-NiCo-LDH-x (x = 2, 4, 6, 8).

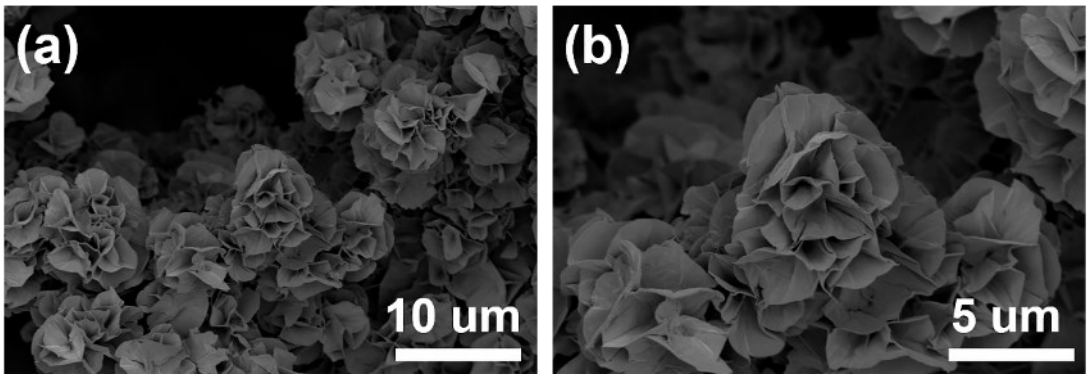

Fig.S7 (a-b) SEM images of the post-catalytic N-NiCo-LDH-6 at different magnifications after the stability test.

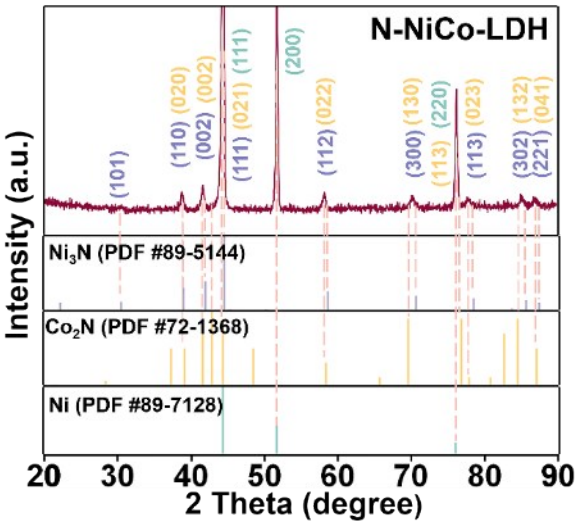

Fig.S8 XRD pattern of the post-catalytic N-NiCo-LDH-6 after the stability test.

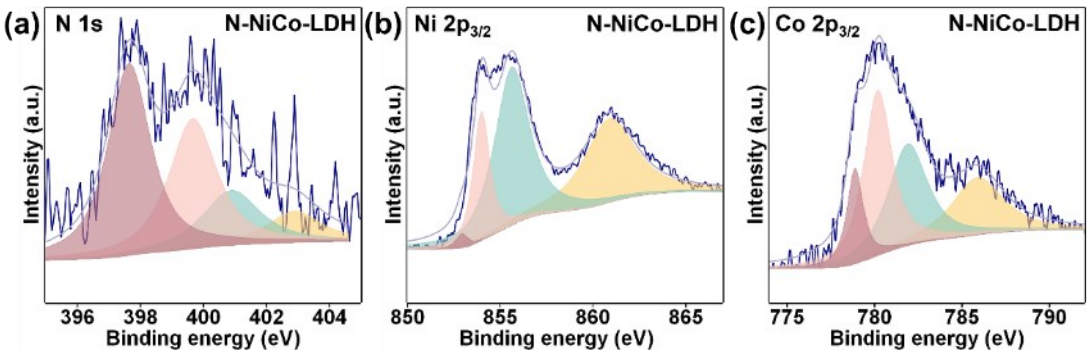

Fig.S9 High-resolution XPS of N 1s spectra (a), Ni $2p_{3/2}$ spectra (b) and Co $2p_{3/2}$ spectra (c) for the post-catalytic N-NiCo-LDH-6 after the stability test.

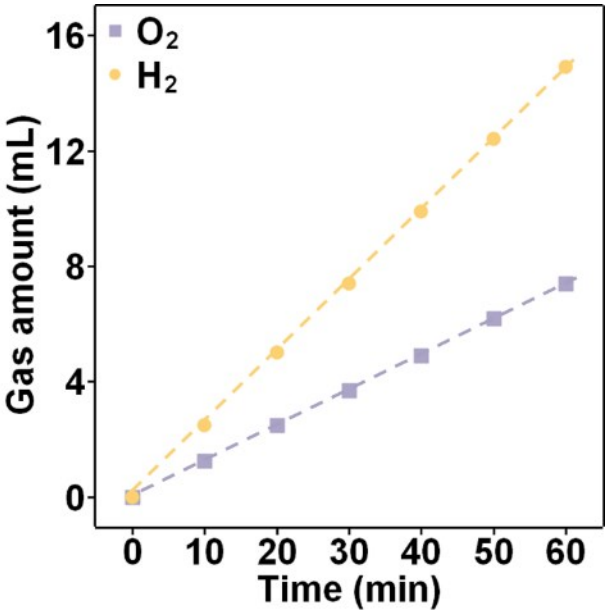

Fig.S10 Electrocatalytic efficiency of overall water splitting for H_2 and O_2 production at 300 $mA \cdot cm^{-2}$ on the N-NiCo-LDH || N-NiCo-LDH couple.

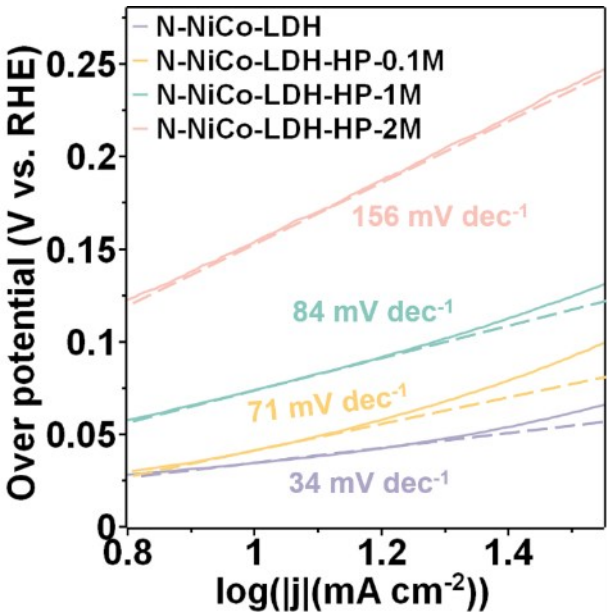

Fig.S11 HER Tafel plots of N-NiCo-LDH-6 (in 0, 0.1, 1, and 2 M dihydrogen phosphate ions).

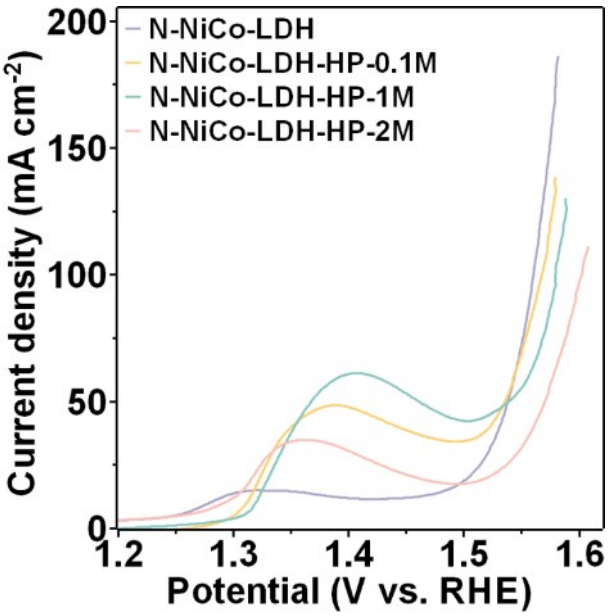

Fig.S12 OER LSV curves of N-NiCo-LDH-6 (in 0, 0.1, 1, and 2 M dihydrogen phosphate ions).

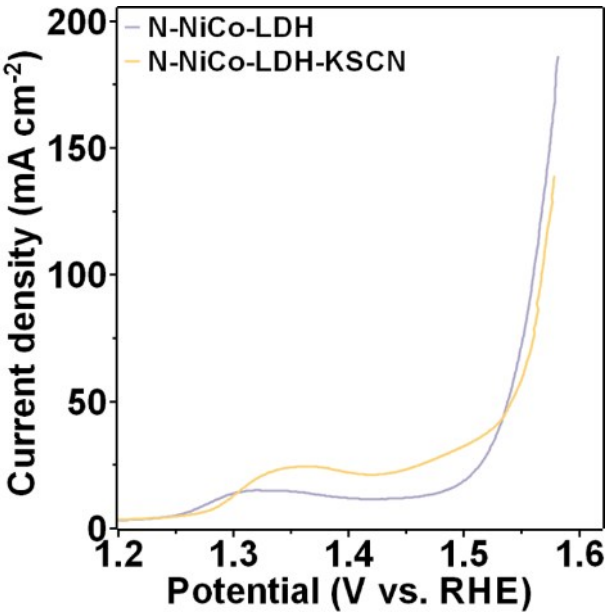

Fig.S13 OER LSV curves of N-NiCo-LDH-6 in 1 M KOH solutions with thiocyanate ions.

3. Supplementary Tables

Tab.S1 Comparison of the HER performance of N-NiCo-LDH-6 with other reported electrocatalysts in 1 M KOH solution.

Catalysts	*Overpotential*	Tafel Slope (mV dec^{-1})	Ref.
N-NiCo-LDH-6	35 mV@10mA cm^{-2}	34	Our work
Ni-BDT-A	80 mV@10mA cm^{-2}	70	*Chem*, 2017, **3**, 122–133.[1]
MoP/CDs	70 mV@10mA cm^{-2}	77.5	*Nano Energy*, 2020, **72**, 104730.[2]
MoS_2/NiS_2 Nanosheets	62 mV@10mA cm^{-2}	50.1	*Adv. Sci.*, 2019, **6**, 1900246.[3]
CoP-MOF	34 mV@10mA cm^{-2}	63	*Angew. Chem. Int. Ed.*, 2019, **58**, 4679–4684.[4]
$Co_{0.97}V_{0.03}SP$	105 mV@10mA cm^{-2}	65	*Adv. Energy Mater.*, 2018, **8**, 1702139.[5]
Ni_3N-VN/NF	64 mV@10mA cm^{-2}	37	*Adv. Mater.*, 2019, **31**, e1901174.[6]
NiFe-LDH	59 mV@10mA cm^{-2}	62.3	*Energy Environ. Sci.*, 2019, **12**, 572–581[7]
MoS_2-confined $Co(OH)_2$	89 mV@10mA cm^{-2}	53	*ACS Nano*, 2018, **12**, 4565–4573.[8]
1T-MoS_2/NiOOH	73 mV@10mA cm^{-2}	75	*Adv. Sci.*, 2018, **5**, 1700644.[9]
CoP/Ni_5P_4/CoP	71 mV@10mA cm^{-2}	58	*Energy Environ. Sci.*, 2018, **11**, 2246–2252.[10]
O-doped Co_2P	101 mV@10mA cm^{-2}	69.4	*Appl. Catal. B Environ.*, 2020, **261**, 118268.[11]
$NiPS_3/Ni_2P$	85 mV@10mA cm^{-2}	82	2019, **13**, 7975–7984.[12]
Se-NiCoP	164 mV@ 100mA cm^{-2}	95	*Nano Energy*, 2021, **81**, 105641.[13]
NiCoP/NPC	128 mV@10mA cm^{-2}	70	*Appl. Catal. B Environ.*, 2021, **283**, 119635.[14]
N-NiMoS	68 mV@10mA cm^{-2}	86	*Appl. Catal. B Environ.*, 2020, **276**, 119137.[15]

Tab.S2 The fitting parameters obtained from the EIS data.

Catalysts	R_s	R_{ct}
N-NiCo-LDH-6	0.84	2.06
NiCo-LDH	1.15	64.44
Ni	1.13	11.37
Pt/C	1.05	1.87

Tab.S3 Calculated conductivity of N-NiCo-LDH-2, N-NiCo-LDH-4, N-NiCo-LDH-6, and N-NiCo-LDH-8.

	N-NiCo-LDH-2	**N-NiCo-LDH-4**	**N-NiCo-LDH-6**	**N-NiCo-LDH-8**
σ (S m^{-1})	0.202	7.012	7.301	6.702

Tab.S4 Calculated TOF of N-NiCo-LDH-2, N-NiCo-LDH-4, N-NiCo-LDH-6, and N-NiCo-LDH-8 at -0.1 V (vs. RHE).

	N-NiCo-LDH-2	**N-NiCo-LDH-4**	**N-NiCo-LDH-6**	**N-NiCo-LDH-8**
TOF (S^{-1})	3.84×10^{-4}	1.04×10^{-2}	1.14×10^{-2}	8.96×10^{-3}

4. Refences

1 C. Hu, Q. Ma, S.-F. Hung, Z.-N. Chen, D. Ou, B. Ren, H. M. Chen, G. Fu and N. Zheng, *Chem*, 2017, **3**, 122–133.

2 H. Song, Y. Li, L. Shang, Z. Tang, T. Zhang and S. Lu, *Nano Energy*, 2020, **72**, 104730.

3 J. Lin, P. Wang, H. Wang, C. Li, X. Si, J. Qi, J. Cao, Z. Zhong, W. Fei and J. Feng, *Adv. Sci.*, 2019, **6**, 1900246.

4 T. Liu, P. Li, N. Yao, G. Cheng, S. Chen, W. Luo and Y. Yin, *Angew. Chem. Int. Ed.*, 2019, **58**, 4679–4684.

5 N. Q. Tran, V. Q. Bui, H. M. Le, Y. Kawazoe and H. Lee, *Adv. Energy Mater.*, 2018, **8**, 1702139.

6 Haijing, Yan, Ying, Xie, Aiping, Wu, Zhicheng, Cai, Lei, and Wang, *Adv. Mater.*, 2019, **31**, e1901174.

7 Z. Qiu, C.-W. Tai, G. A. Niklasson and T. Edvinsson, *Energy Environ. Sci.*, 2019, **12**, 572–581.

8 Y. Luo, X. Li, X. Cai, X. Zou, F. Kang, H.-M. Cheng and B. Liu, *ACS Nano*, 2018, **12**, 4565–4573.

9 X. Zhang and Y. Liang, *Adv. Sci.*, 2018, **5**, 1700644.

10 I. K. Mishra, H. Zhou, J. Sun, F. Qin, K. Dahal, J. Bao, S. Chen and Z. Ren, *Energy Environ. Sci.*, 2018, **11**, 2246–2252.

11 T. L. [Luyen Doan, D. T. Tran, D. C. Nguyen, H. [Tuan Le, N. H. Kim and J. H. Lee, *Appl. Catal. B Environ.*, 2020, **261**, 118268.

12 Q. Liang, L. Zhong, C. Du, Y. Luo, J. Zhao, Y. Zheng, J. Xu, J. Ma, C. Liu and S. Li, *ACS Nano*, 2019, **13**, 7975–7984.

13 Y. Liu, Q. Feng, W. Liu, Q. Li, Y. Wang, B. Liu, L. Zheng, W. Wang, L. Huang, L. Chen, X. Xiong and Y. Lei, *Nano Energy*, 2021, **81**, 105641.

14 M. Yi, B. Lu, X. Zhang, Y. Tan, Z. Zhu, Z. Pan and J. Zhang, *Appl. Catal. B Environ.*, 2021, **283**, 119635.

15 C. Huang, L. Yu, W. Zhang, Q. Xiao, J. Zhou, Y. Zhang, P. An, J. Zhang and Y. Yu, *Appl. Catal. B Environ.*, 2020, **276**, 119137.